Project Report for MOD8 by Group 7

Design of a Pen plotter

Authors -

Yorick Smit	Krijn Schouten	Bram Kieskamp
1850814	1499408	1856073
Wouter Dobbenberg	Thomas Dommerholt	
1722980	1866141	

Supervisor -

Dr. I.S.M. Khalil

University of Twente
2019/06/28

Contents

Introduction **2**

1 Requirements and specifications **2**

2 Leaf spring design **2**

3 Mechanical design **4**

4 Controller theory **5**

5 Controller design for the nominal model **6**

6 Testing the Simulated model **8**

7 Physical model **10**

8 Validation **11**

References **13**

Appendices **14**

A Measurement plan - Steady state response **14**

B Measurement plan - Frequency response **15**

C Initial Design **16**

D High order TF [SPACAR] **17**

E Simulated model bode diagrams **17**

F Simulink model **18**

Introduction

Before the prevalence of ink-jet printers, pen plotters were used to construct various line drawings. Although pen plotters nowadays have been replaced, technologies developed for these devices are still used in other areas such as 3D printing.

In this project, a pen plotter is designed to follow a given trajectory with certain specifications (see next section). To do this, principles from dynamics and systems & control are used.

1 Requirements and specifications

The system has to perform according to certain requirements. The hardware also has certain specifications and limitations that have to be taken into account. These specifications and limitations will be presented in this section.

1.1 Requirements

Both stages of the setup, the X-stage (or cart-stage) and Y-stage (or pen-stage), have to meet+ the requirements. These requirements are listed below:

- A combined accuracy of 0.25 mm.
- X-stage range of 150 mm.
- Y-stage range of 10 mm.
- Y-stage spatial period of 15 mm along the X-axis.
- The minimum velocity of the X-axis is 0.20 m/s.

In addition to the mentioned requirements, the velocity of the X-axis, and thus the system, should be maximized.

1.2 Reference trajectory

The specified accuracy will be measured using the sensors. It will also be visualised by moving back and forth along the trajectory with a pen. This trajectory is presented in Figure 1. In this figure the profile along the X- and Y-axis is displayed as well as the velocity, acceleration and jerk profiles.

1.3 Relevant specifications of available hardware

Relevant specifications and limitations of the available hardware are listed here:

Motor - Maxon Rotatie AC-motor 323772

- Pulley radius: 22 mm

Rotary encoder - Maxon MILE 800–6400 CPT 6400

- Counts: 25600 counts/turn

VCM - AVM30-15

- Stroke: 15 mm

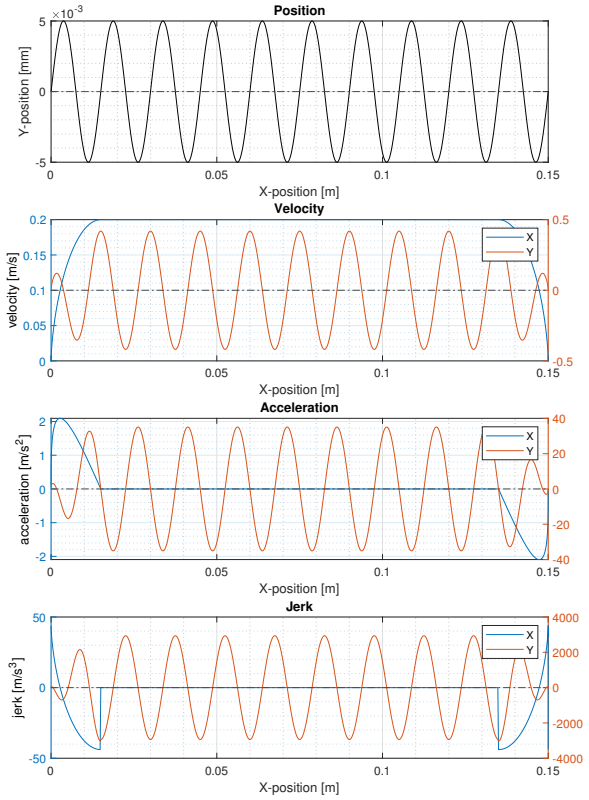

Figure 1: Reference trajectory

- Mass: coil 36 g, core 95.6 g
- Peak force: 29.4 N at 40 V
- Continuous force: 4.63 N

Linear encoder - RLS RLB 13B

- Counts: 8192 counts/2 mm
- Mass readhead: 0.46 g
- Maximum separation distance: 0.1-0.8mm

Amplifier - Custom built

- Voltage output to VCM: +/-24 V, +/-100% PWM (restricted at 25% PWM)
- Current output to motor: 3.75A (restricted)

Leafsprings - Lasercut [1]

- Available thickness: 0.2, 0.3, 0.4, 0.5 and 0.6 mm.
- Maximum length: 330 mm
- Maximum width: 100 mm
- E-modulus: 200 GPa
- Tensile strength: 500-750 MPa

2 Leaf spring design

An important factor which influences the performance of the system are the leaf springs. The stiffness of the leaf springs should be chosen such that the VCM (Voice Coil Motor) has enough force to reach its maximum required excitation, as well as an appropriate amount of

stiffness for the given acceleration profile, and enough stiffness in the direction of the parasitic modes.

In this section an analysis of the leaf springs will be performed in order to calculate the maximum stiffness, ideal geometry, as well as the maximum stress that occurs in the leaf spring.

2.1 Equivalent stiffness

The leaf springs are used for a straight (parallel) guiding. A schematic overview can be seen in Figure 2. The leaf springs can be considered clamped on both sides. This results in an S-shaped deflection mode. To calculate the stiffness, the leaf spring is cut at $l = l/2$, with deflection $\delta = \delta/2$. Each half can be considered as a free-fixed beam.

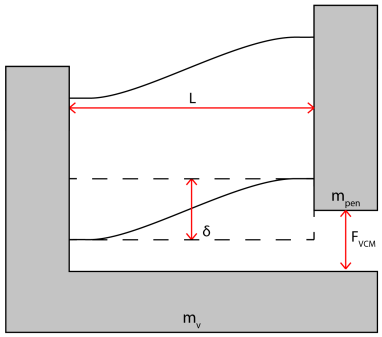

Figure 2: Schematic overview of the pen stage with leaf spring straight guide

With the beam deflection formulas, this yields the stiffness of each half of the leaf spring and a single leaf spring:

$$k = \frac{dF}{d\delta} = \frac{12EI}{l^3} \quad \text{with} \quad I = \frac{1}{12}bh^3 \tag{1}$$

$$k = \frac{Ebh^3}{l^3}, \tag{2}$$

where b and h are the width and thickness of the leaf spring, E is the Young's modulus, and I the moment of inertia.

The equivalent spring stiffness for the two complete leaf springs in parallel configuration, k_{eq}, can be written as twice the stiffness of a single leaf spring.

2.2 Dimensional flexure analysis

Several configurations are possible to acquire a certain stiffness. An analysis on the parameters can show how changing parameters affects the stiffness. From Equation 1 it can be seen that length and thickness go by the power of three. An increase of 26% of these parameters will change the result by a factor 2. The width will have to be doubled for the same effect.

2.3 Maximum stiffness of the flexure

Considering the model for the pen stage, the maximum stiffness of the leaf springs can be determined.
The force by the springs can be calculated as follows:

$$F_{2leafs}(\delta) = 2\frac{Ebh^3}{l^3}\delta \tag{3}$$

The force balance is then:

$$F_{2leafs} = F_{vcm} + F_{net} \tag{4}$$

At the maximum excitation, the VCM can counteract the leaf spring force to reach the desired acceleration. The stiffness at which this occurs can be found using the following equation:

$$k_{eq,max}\delta_{max} = F_{vcm,max} + m_{pen}a_{y,max} \tag{5}$$

The maximum acceleration of the pen stage is 35 m/s^2 (Figure 1). The mass of the redesigned pen stage (Section 3) is 0.24697 kg. From the datasheets, a maximal actuator force of 29.40 N at 40.88 V can be found, but the amplifier used is limited to using 24 V and a PWM duty-cycle of 25%. The relation between force and voltage is linear and can be interpolated to be 4.32 N at 6 V. From the equations above a maximum equivalent stiffness ($k_{eq,max}$) of 2.3855 N/mm is obtained.

2.4 Design of the leaf springs

With the design parameters of the leaf spring both the eigenfrequencies as well as the directional stiffnesses can be influenced. In order to achieve the required performance of the pen plotter, these two parameters should be analysed.

The stiffness of the leaf springs should be low enough to allow the pen stage to reach the required acceleration (Subsection 2.3). The leaf spring should also be strong enough to withstand the stresses on the material. This will be checked after the redesign (Subsection 2.5). Furthermore the first eigenfrequency of the system (in the direction of motion) should be just beyond the operating frequency of 13.3 Hz (see Figure 1). In that case the input force from the VCM will be lower, which is desirable. The first parasitic frequency should be as high as possible so that resonance is unlikely to occur and at least four times bigger than the cross-over frequency (Section 5.2).

It follows from the constraints that the leaf spring should be both thin (low first eigenfrequency) and wide (high first parasitic frequency/second eigenfrequency), whilst not exceeding the tensile stress. This results in a spring with a low stiffness in the primary direction of motion and a high stiffness in the secondary (parasitic) direction of motion.

The leaf springs were designed considering all information above. The dimensions are shown in Figure 3. The dimensions of the leaf springs are l= 50 mm, b= 8 mm

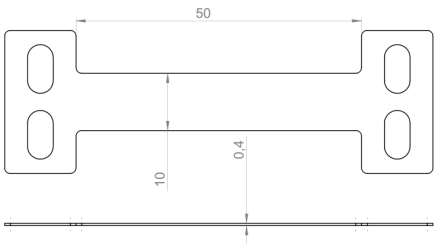

Figure 3: Redesigned leaf springs

and $h = 0.4$ mm. The stiffness for this configuration is 2.048 N/mm. The eigenfrequency of the pen stage with these leaf springs is $\sqrt{k_{eq}/m_{pen}} = 15.46$ Hz.

2.5 Maximum stress of the flexures in relation to its properties

2.5.1 Bending stress

The bending stress for a 2-dimensional element can be calculated using the following formula:

$$\sigma_b = \frac{My}{I} \quad \text{with} \quad I = \frac{1}{12}bh^3, \tag{6}$$

where M is moment, I the moment of inertia of a rectangular cross section and y the distance to the neutral line.

The maximum bending stress can be observed at the outer edges of the element. The largest force, and maximum stress can be found in the direction of movement. The neutral plane is normal to the thickness of the leaf spring. For this case the equation can be rewritten to:

$$\sigma_{bending,max} = \frac{M_{max}\frac{1}{2}h}{I} = \frac{6M_{max}h}{bh^3}, \tag{7}$$

where M_{max} is the maximum moment occurring in the leaf spring. Using Equation 3:

$$M_{max} = \frac{Pl}{2} = \frac{\frac{1}{2}\cdot F_{2leafs,max}\cdot l}{2} = \frac{Ebh^3}{2l^2}\delta, \tag{8}$$

with P the perpendicular force on the equivalent bar length $\frac{1}{2}l$. This gives the final equation for the maximum bending stress:

$$\sigma_{bending,max} = \frac{3Eh\delta}{l^2} \tag{9}$$

Which results in a maximum bending stress of 480 MPa.

2.5.2 Shear stress

The maximum shear stress is obtained using Equation 10 [2].

$$\sigma_{shear,max} = \frac{3V}{2A} \tag{10}$$

Rewriting this using Equation 3:

$$\sigma_{shear,max} = \frac{3Ebh^3}{2l^3}\delta\frac{1}{bh} = \frac{3Eh^2}{2l^3}\delta \tag{11}$$

This results in a shear stress of 1.92 MPa, which is negligible considering the bending stress.

2.5.3 Gravity induced bending stress

Lastly, there is a bending stress on the leaf springs as caused by the gravity. This is calculated in a similar way to the maximum bending stress as caused by the VCM:

$$\sigma_{bending,gravity} = \frac{M_{gravity}\frac{1}{2}b}{I} = \frac{6M_{gravity}b}{hb^3} \tag{12}$$

$$M_{gravity} = \frac{Pl}{2} = \frac{\frac{1}{2}gm_{pen}l}{2} \tag{13}$$

$$\sigma_{bending,gravity} = \frac{6gm_{pen}l}{4hb^2} \tag{14}$$

This gives a bending stress of 2 MPa.

This means that, in this case, the maximum stress that occurs in the leaf spring is 480 MPa, which is within the tensile strength of the material (Section 1.3).

3 Mechanical design

A design of the setup (Figure 4 was made based on an older setup (Appendix C). The design elements of the setups will be compared.

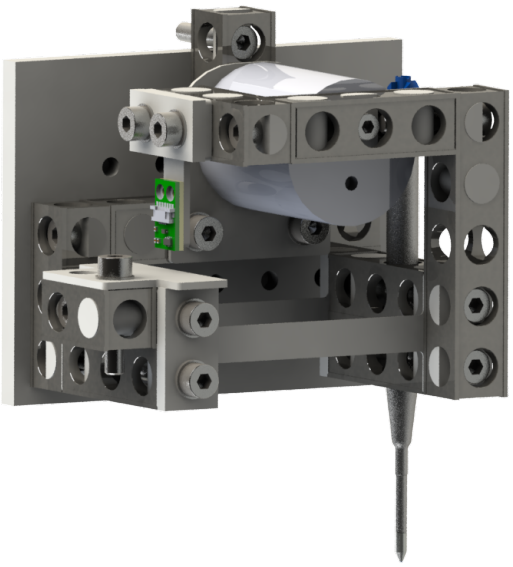

Figure 4: Designed test setup

3.1 Flexures

3.1.1 Degrees Of Freedom

A leaf spring constrains 3 Degrees Of Freedom (DOF), 2 in-plane translations and the out-of-plane rotation. Adding a second leaf spring in a parallel configuration will constrain two additional DOF, the in-plane rotations. The remaining DOF is the movement direction, which is the only required DOF.

Use of two leaf springs will result in an overconstrained system. One of the springs should be notched, but this was deemed unnecessary, since the exact forces in the separate leaf springs were not critical to the performance of the system.

3.1.2 Orientation of the leaf springs

The leaf springs are fixed in the same orientation. Fixing the springs vertically caused problems with the pen. The shortening effect would cause the pen to lose contact with the paper. The shortening effect of the leaf springs is 0.3 mm for the maximum excitation (Equation 15).

$$u = -0.6\frac{\delta^2}{l} \tag{15}$$

3.2 VCM location

The VCM was kept close to the centre of compliance of the leaf springs so the forces would mostly work in the moving direction and a minimal amount of unwanted moments are present.

3.3 Sensor location

The sensor is mounted in the same orientation as it was before. The other plane was not an option since the shortening of the leaf springs would be on the boundaries of the distance range of the sensor and give inaccurate readings. The position of the sensor did change.

3.4 Co-location of the sensors

The new design is co-located instead of non co-located, as the sensor is mounted on the same plane of motion as the VCM. The sensor measures in the same plane of motion as the actuator. This is important for the stability of the system, since no measuring errors are introduced by the parasitic motions of the pen stage.

3.5 Mass of the moving pen stage

The total mass mounted to the cart is 0.41628 kg. The mass of the "hanging" part of the stage had a mass of 0.370 kg, whereas the initial redesign has a "hanging" mass of 0.247 kg. A lower mass means a lower inertia which causes the system to be more responsive to forces.

4 Controller theory

To control the motion of the pen plotter, two controllers will have to be used. One for each axis of the pen plotter. They both follow the same structure, but have different values.

4.1 Controller type selection

There are several controllers K available to control the cart en pen system. mainly there are 4 types of controllers; P, PI, PD and PID. Both the pen plotter and cart stage will be controlled by a PID controller. The PID controller will provide a robust control, which means it will be able to suppress certain (dynamic) disturbances adequately and at the same time satisfies all other dynamic specifications.
The entire controller model of both plants can be found in Appendix F.

4.2 PID Control

In a block diagram the serial PID controller (K) represents the following transfer function:

$$K_{PID}(s) = k_p \cdot \frac{(s\tau_z + 1)(s\tau_i + 1)}{s\tau_p + 1} \tag{16}$$

The parameters used to tune the controller are:

$$k_p = \frac{m_{eq}\omega_c^2}{\sqrt{(\frac{1}{\alpha})}} \tag{17}$$

$$\tau_z = \frac{\sqrt{\frac{1}{\alpha}}}{\omega_c} \tag{18}$$

$$\tau_i = \beta \cdot \tau_z \tag{19}$$

$$\tau_p = \frac{1}{\omega_c \cdot \sqrt{\frac{1}{\alpha}}} \tag{20}$$

From the values for ω_c, α and β the final control parameters can be determined.

4.3 Feed forward

To decrease the cross-over frequency, feed-forward can be applied. This does not influence the stability of the system. The complete block diagram of the system including feed-forward can be seen in Figure 5. The controller is denoted by K, the plant by G and the feed-forward by F.

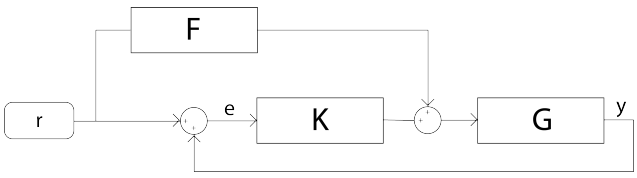

Figure 5: Overall controller structure

4.4 Error and cross-over frequency

The maximum absolute error of the pen plotter is given in the requirements (0.25 mm). An absolute error includes a contribution from the cart-stage and the pen-stage. The error per stage can be calculated as:

$$e_t^2 = e_{pen}^2 + e_{cart}^2 = 0.25^2 \tag{21}$$

The maximum error for each of the stages were chosen to be equal (0.177 mm).

The servo error is the difference between the behaviour in time of the reference and the controlled system. The equations to predict the maximum servo error are derived in the following section.

4.4.1 Maximum servo error in time domain as function of cross-over frequency

The reference trajectory will give the function for r and its derivatives. For the cart stage, this is r_x and for the pen-stage this is r_y. The outputs of these stages are x and y respectively.

From the block diagram in Figure 5, the symbolic transfer function can be derived:

$$y(s) = (r_y(s) - y(s)) \cdot G(s)K(s) + G(s)F(s) \cdot r(s) \tag{22}$$

rewriting with $e_y(s) = r_y(s) - y(s)$ gives

$$\frac{e_y(s)}{r_y(s)} = \frac{1 - G(s)F(s)}{1 + G(s)K(s)} = (1 - \gamma(s)) \cdot S(s) \tag{23}$$

where $\gamma = G(s)F(s)$

The same is true for the pen stage with e_x, x and r_x.

For full compensation, separate feed forward are used for the acceleration (to compensate the mass), velocity (damping) and position (stiffness). The factors g_i are used for the uncertainty in the plant parameters. This value typically ranges $0.8 < g_i \leq 1$. The feed forward transfer function is then:

$$F(s) = g_1 \frac{m}{k_m} + g_2 \frac{d}{k_m} + g_3 \frac{k}{k_m} \tag{24}$$

The low frequency similarity of S, S_{LF}, with feed forward:

$$S_{LF} = \frac{(1 - g_1)s^3 + (1 - g_2)\frac{d}{m}s^2 + (1 - g_3)\frac{k}{m}s}{(\frac{k}{m} + (1 + \frac{1}{\beta})\sqrt{\alpha}\omega_c^2)s + \frac{1}{\beta}\alpha\omega_c^3} \tag{25}$$

The relation between error and cross-over frequency in time domain is

$$e_{LF}(t) = k_j(1-g_1)\cdot\dddot{r}(t) + k_a(1-g_2)\cdot\ddot{r}(t) + k_v(1-g_3)\cdot\dot{r}(t) \tag{26}$$

The parameters are:

$$k_j = \beta \cdot \frac{1}{\alpha \cdot \omega_c^3} \tag{27}$$

$$k_a = \beta \cdot \frac{\frac{d}{m}}{\alpha \cdot \omega_c^3} \tag{28}$$

$$k_v = \beta \cdot \frac{\omega_1^2}{\alpha \cdot \omega_c^3} \tag{29}$$

When feed forward would not be used, $F(s)$ and thus $\gamma(s)$ will be zero. This results in g_i to be zero and in that case, the cross-over frequency will increase.

5 Controller design for the nominal model

To design the controllers, a step by step approach is applied. The approach applied in three different sections (5 to 7). Each section describes a different resolution of the Mechatronics Control Theory. The following steps were followed:

- First of all the system specifications are recalled from sections 1.3 to 3.5.
- Based on the nature of the system, the controller architecture is determined.
- The desired cross-over frequency is calculated based on the system specifications and architecture.
- The tuning-values of the controller are then determined using the cross-over frequency and control parameters α and β.
- The stability is tested of the tuned open-loop system by iterating through different values of α and β in the previous step.
- When a stable and well behaved system is found, the continuous system is discretized.
- The controller gains are re-tuned to satisfy the system specifications for the discretized model.
- The new controller parameters are applied to the real plant.
- The controller gains are re-tuned to compensate for the inaccuracy of the nominal model.
- Finally the system is compared to the theory.

A simple analysis of the system is required. This simple time-continuous second-order nominal representation of the system will form the basis for the more realistic discrete multiple order system. From this nominal model the first open loop Bode plots can be created which give the first information about the stability of the system.

5.1 IPM and TF

In order to evaluate the stability of the system. both the controller and the mechanical plant have to be modelled. The Ideal Physical Model (IPM) can be seen in Figure 6. From the IPM the nominal transfer functions can be derived. Both the cart stage and the pen stage plant will be modelled as second order systems (Equation 30 and Equation 31).

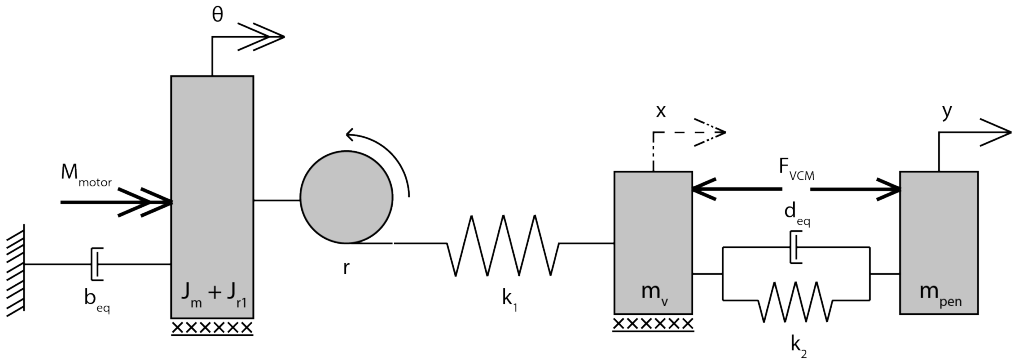

Figure 6: IPM of the pen plotter setup

$$G_{cart}(s) = \frac{\frac{K_{m,cart}}{J}}{s^2 + \frac{b}{J} \cdot s} \tag{30}$$

$$G_{pen}(s) = \frac{\frac{k_{m,pen}}{R * m_{pen}}}{s^2 + \frac{d}{m_{pen}} \cdot s + \frac{k}{m_{pen}}} \tag{31}$$

The values for J, c and b were determined through experimentation. The values for m, k and d were calculated with Equations 32, 33 and 34.

$$m = \sum_{i=1}^{x} n_i \cdot m_i \tag{32}$$

$$d = \frac{k_{m,pen}^2}{R} \tag{33}$$

$$k = \frac{2Ebh^3}{l^3} \tag{34}$$

where x equals the number of unique parts. n equals to the numbers of parts of each unique part.

It should be noted that the cart stage stiffness k_1 cannot be measured. Therefore k_1 can be considered zero and the belt is considered infinitely stiff. The resulting values can be found in Table 1.

From now on the following terms will be used in this report: $J = J_m + J_{r1}$, $k = k_2$ and $b = b_{eq}$.

Term	Value	Unit
J	0.00105	$[kg/m^2]$
b_{eq}	0.00625	$[Ns/rad]$
c_{eq}	0	$[N/rad]$
$k_{m,cart}$	0.0705	$[N \cdot m/sqrt(W)]$
m_{pen}	0.2469	$[kg]$
d	0.5176	$[Ns/m]$
k	2048	$[N/mm]$
$k_{m,pen}$	2.30	$[N/sqrt(W)]$
R	10.22	$[\Omega]$

Table 1: Values for stiffness, damping, mass en inertia

5.2 Cross-over frequency

The cross-over frequency was calculated with Equation 26. In this equation, the maximum allowed error of 0.177 mm, and the trajectory values at maximum error are used, which is at $t = 0.0338$ s. This time-instance was used, as the velocity here is at maximum. Inserting Equations 27, 28 and 29 with the chosen parameters of α and β gives the cross-over frequencies. The frequencies for both of the stages are noted in Table 2.

Stage	α	β	$\omega_c\ (Hz)$
Cart	0.1	14.0	38
Pen	0.1	1.5	47

Table 2: Cross-over frequencies

5.3 Control parameters

From the equations from Section 4.2, the PID parameters can be obtained. These values can be seen in Table 3. Since all the plant parameters are known, there is no uncertainty and the values for g_i are 1, with the exception of g_3 of the cart stage, which is 0 since we have not modelled any stiffness for the cart stage.

Parameter	Cart stage	Pen stage
k_p	272.40	29988
τ_z	0.0131	0.0108
τ_i	0.1837	0.0161
τ_p	0.0013	0.0011

Table 3: PID values for the cart and pen controllers

From this the open loop Bode plots can be made to check the stability of the system. The system is stable if the phase margin is less than ± 180 degrees at the cross-over frequency. The Bode plots of these nominal stages can be seen in Figure 12 (cart) and Figure 13 (pen) in Section 6.

6 Testing the Simulated model

The model described in Section 5 is not an accurate representation of reality. The real controller for the pen plotter is digital and therefore cannot respond continuously. This means that the controller and plant have to be discretized. SPACAR can be used to analyse the physical model which can be used in simulations.

6.1 Discretized controller

The controller is not time-continuous, but discretized. It uses digitally sampled signals, sampled at 2000 Hz. This means that the highest frequency the controller can reliably measure is 1000 Hz (half the sample frequency). Frequencies higher than this frequency will be read incorrectly and cause aliasing. These unwanted higher frequencies can be removed by a low-pass filter. In practice, the sampling frequency should be 20-50 times the cross-over frequency ω_c. From this it can be concluded that a sampling frequency of 2000 Hz is reasonable, given the values for ω_c of the discretized controller.

A discretized controller also induces a delay in the signal, which in turn effects the stability of the system. The delay is caused by a poor reconstruction of the signal due to the randomness of the sampling time in relation to the measured signal. This effect can be seen in Figure 7 [3].

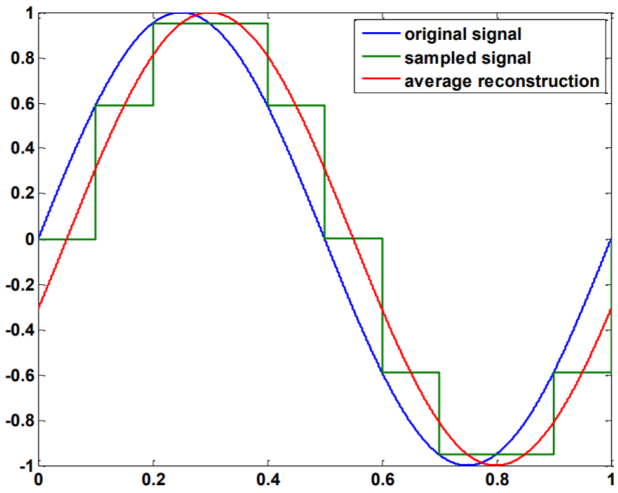

Figure 7: Delay induced by the reconstruction of the sampled signal.

This delay is part of the open-loop Bode plot, so a reduction of the phase margin can be observed. This means the discretization of the controller has a negative impact on the stability.

6.2 Parasitic modes and mode shapes

SPACAR was used to analyze the parasitic modes of the design. The first two parasitic modes are shown in Figure 8. Table 6.2 contains the frequencies of these

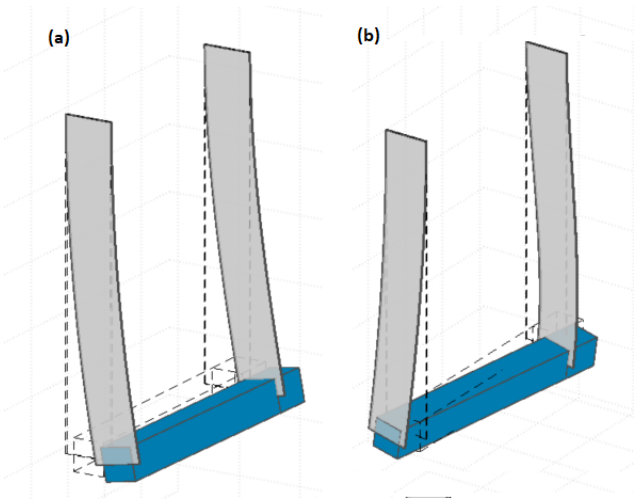

Figure 8: Motion of the flexures of the first parasitic mode (a) and the second parasitic mode (b)

parasitic modes. Both of these parasitic mode shapes appear at a sufficiently high frequency (4x the cross over frequency).

Parasitic mode	Freq	Figure
1^{st}, bending in width direction	193.8 Hz	8a
2^{nd}, rotation around z-axis	379.6 Hz	8b

Table 4: Parasitic Modes

6.3 Higher-order model from SPACAR

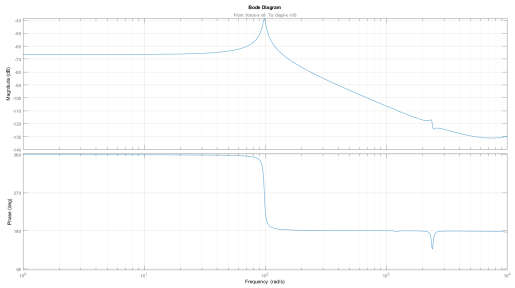

Figure 9: Bode plot SPACAR pen stage

The model of the redesigned pen stage in SPACAR is used to get an more accurate evaluation of the system. A SolidWorks representation as well as the spacar representation of the model can be seen in Figure 10. This model has two leaf springs, a point mass at the center of gravity, and a force on the structure at the location of the VCM. These are connected using weightless and infinitely stiff elements. The location of the center of mass and the mass itself were evaluated using SolidWorks.

SPACAR shows that the eigenfrequency in the direction of excitation is 15.7 Hz. This is similar to the value calculated in Section 2.4.

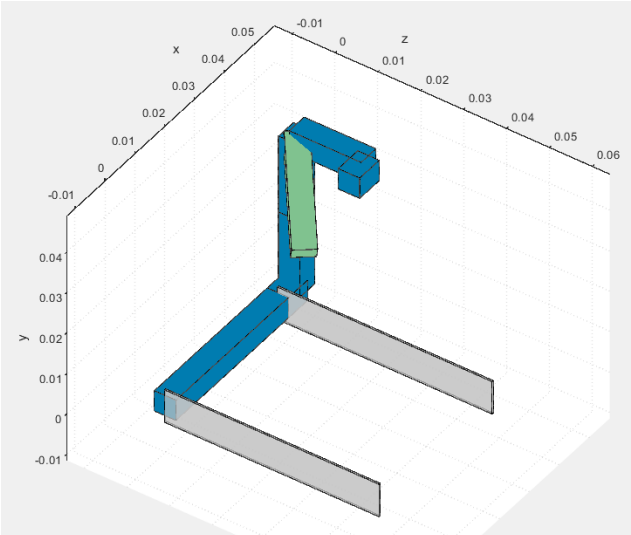

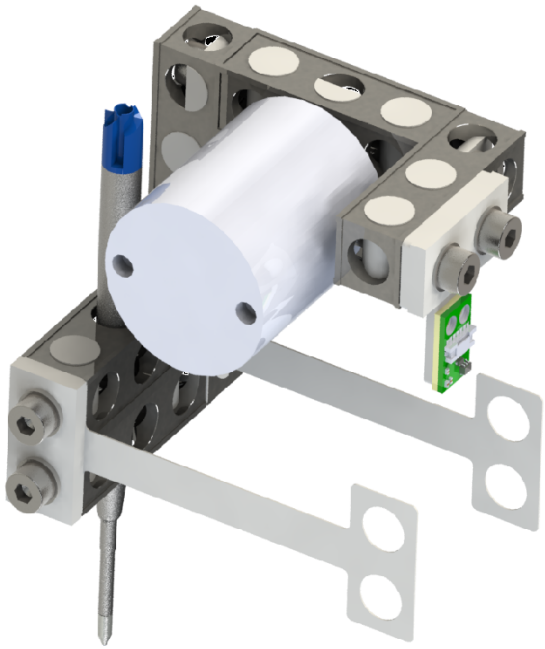

Figure 10: SPACAR model and render of the redesign in the same perspective

The transfer function of the modelled system from SPACA was exported to SIMULINK. The function is shown in Appendix D, Equation 35. The Bode plot of this transfer function without controller or feed forward is shown in Figure 9. A larger version of this figure can be found in Appendix E, Figure 29.

6.4 Controller

The blue line in Figure 11 represents the system including controller and feed forward. A larger version of this figure can be found in Appendix E, Figure 30. The controller parameters used to acquire this diagram are noted in Table 3. These are the same values as used for the nominal model.

To account for inaccuracies in the measured plant parameters, the uncertainty variables g_i of both plants are set to 0.8, with the exception of the g_3 for the cart stage, which is 0. This has been done because an additional error has been introduced by the difference between the variables introduced in Table 1 and the transfer function found by SPACAR in Section 6.3.

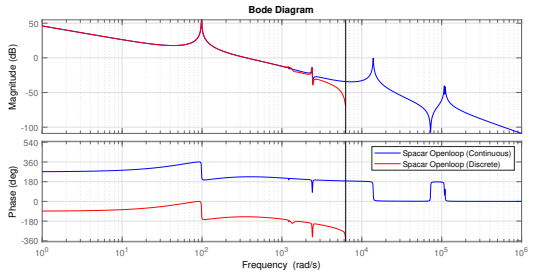

Figure 11: Bode diagram of the simulated plant including controller and feed-forward

6.5 Bode open loop stability

In this section both the nominal (blue) and discretized (red) Bode plot of the open loop can be seen for both the cart stage Figure 12 and pen stage Figure 13.

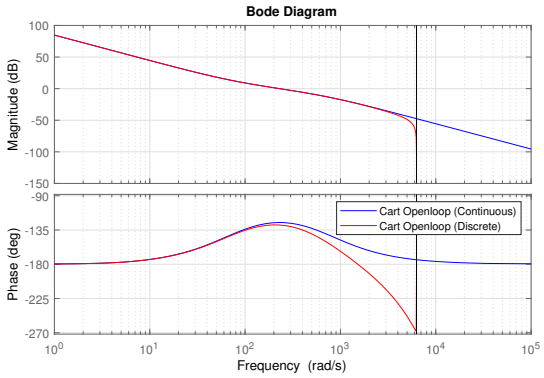

Figure 12: Comparison (nominal in blue, discretized in red) of the open loop Bode plot of the cart stage

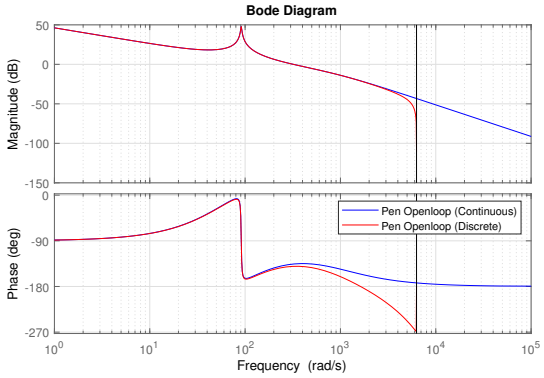

Figure 13: Comparison (nominal in blue, discretized in red) of the open loop Bode plot of the pen stage

6.6 Nyquist closed loop stability

In order to determine the closed loop stability of the system, two Nyquist diagrams are made for the continuous open loop system, Figure 14 for the pen stage and Figure 15 for the cart stage. These diagrams are related to the closed loop stability since for the closed loop, the poles of the open loop system become zeros and vice versa. A system is considered unstable if there is a pole in the RHP (Right Half Plane). So if there is no encirclement of the point -1 (counter clockwise in the open loop), the closed system can be considered stable since this means that there are no poles in the RHP for the closed loop system.

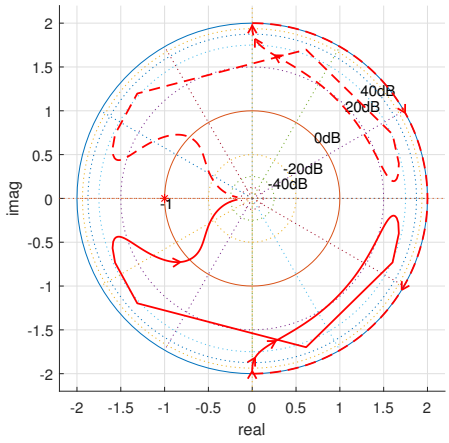

Figure 14: Logarithmic closed-loop nyquist diagram of the pen stage

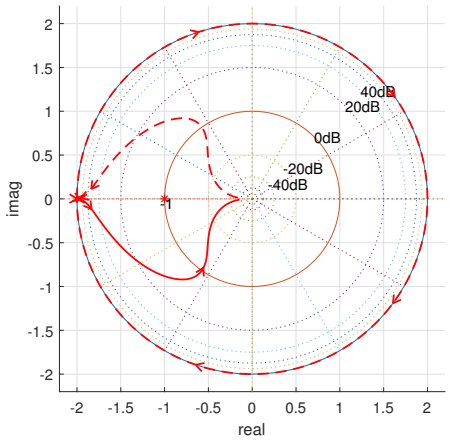

Figure 15: Logarithmic closed-loop nyquist diagram of the cart stage

The Nyquist diagrams were made with help from files on Mathworks File-Exchange [4]. These files have solely been used for visual improvements of the original nyquist diagrams.

6.7 Trajectory and simulated error

After running the simulated plant the the simulated trajectory (Figure 16) and simulated error (Figure 17) were plotted. This model does not have the hardware limitations of the real plant, and as such it is able to provide as much force as is needed.

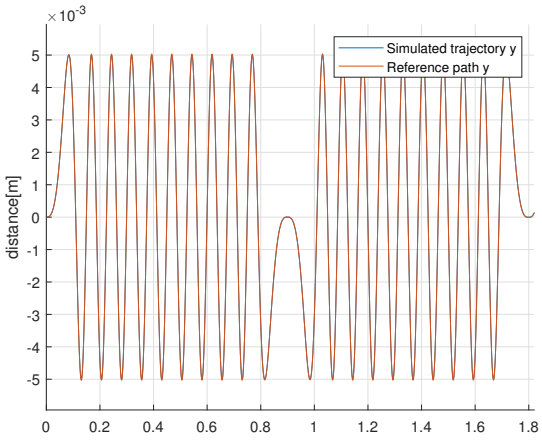

Figure 16: Simulated trajectory

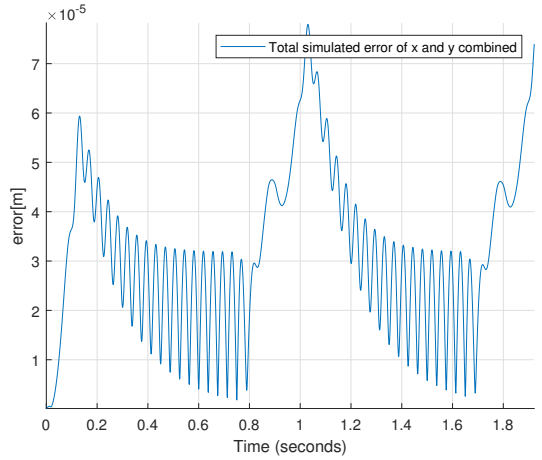

Figure 17: Simulated error

7 Physical model

In the final step the controller designed in Section 6 will be implemented on the physical controller. The systems performance will be evaluated and the PID controller values in Table 3 will be finetuned to reach the requirements stated in section 1.1. Since the system parameters from Section 5 and Section 6 are not fully accurate, two more test will be performed. A steady-state test to determine if the system responds linearly, and a frequency response test, to determine if the system responds similarly to the model from Section 6.

7.1 Linearity

To check the linearity of the pen stage the static gain was evaluated. This was done by executing a steady state response test of the system. The measurement plan of this procedure can be found in Appendix A. The values of the excitation for different voltages were plotted (blue dots) against time and later approximated with an polyfit (blue line) in Figure 18. This graph can be compared to the graph derived from the values from the datasheets of the manufacturer (green line). There is a 10 % difference in the derrivative of these lines. This is quite a difference but the controller used will compensate for this. In Figure 18 the error between the measured excitations and the polyfit is plotted against voltage as well, shown as the red graph. This error is on average less than 1%. This is significantly small, and therefore the system can be assumed to be linear.

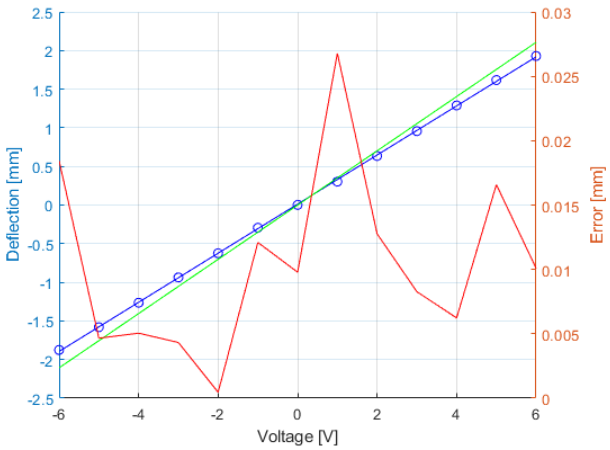

Figure 18: Linearization

7.2 Frequency response

The frequency responses of the cart and pen stage can be seen in Figure 19 and Figure 20. The measurement plan for determining these FRFs can be seen in Appendix B. It can be observed that the phase of the cart stage has shifted upwards by 180 degrees. The pen stage response has a higher gain than the model.

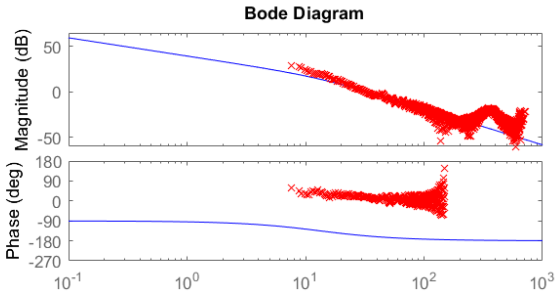

Figure 19: Open loop Bode diagram of the physical cart stage

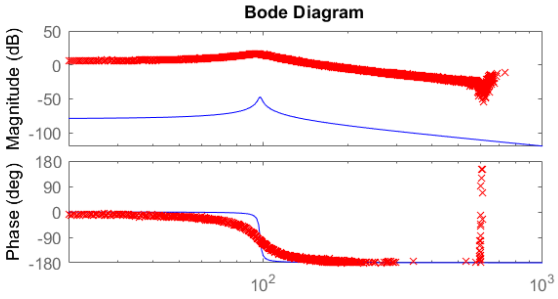

Figure 20: Open loop Bode diagram of the physical pen stage

7.3 Feed forward

Since it is not possible to exactly know the variables for the feed forward in the real plant, the uncertainty factors have to be adjusted. In the physical controller the variable g_3 is 0.8 for the pen stage, but 0 for the cart stage (no feed forward). g_1 and g_2 are set to 0.8 (for both the pen and cart stage).

8 Validation

In this section the performance of the physical model will be compared to the simulated model. The performance will also be compared against the specifications.

8.1 Comparison to simulated model

As can be seen when comparing Tables 2 and 3 with Table 5, mostly the same PID control variables have been used in the real plant as in the simulated plant. The only exception are the τ_z values, which have been lowered by 25% in the real plant to improve the results. The final controller parameters can be seen in Table 5. α and β have remained the same as the simulated plant.

Parameter	Cart stage	Pen stage
k_p	272.40	29988
τ_z	0.0098	0.0081
τ_i	0.1837	0.0161
τ_p	9.8414e-04	8.0681e-04

Table 5: PID values for the discretized cart and pen controllers

8.2 Meeting the requirements

The requirements for the system were listed at the beginning of the report in Subsection 1.1.

The maximum combined error was well within the requirements except for a small part of the trajectory, as can be seen in Figure 23. The accuracy was not sufficient for the period of the trajectory where the pen has to accelerate from standstill and where it has to decelerate. At this part of the trajectory, the voltage output maxed out at 6 V (25% PWM), which reached

a displacement lower than 5 mm. To decrease the error here, the maximum (restricted) voltage output of the amplifier could be increased.

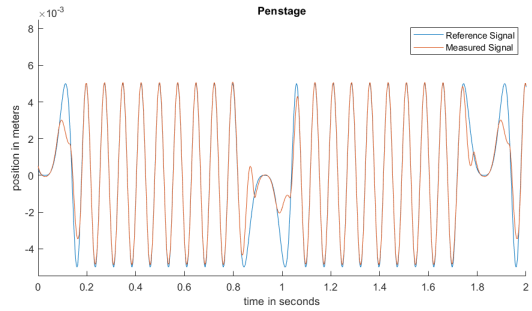

Figure 21: Measured signal of the pen stage compared to the reference signal

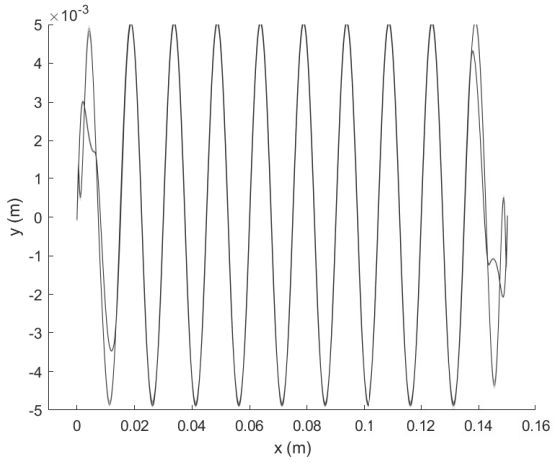

Figure 22: Measured trajectory of the system

From the measurements on the actual followed trajectory (Figure 23) it can be seen that, during the steady state motion, the displacement of 5 mm on both sides are met within the accuracy margin.

When comparing the real results to the simulated models. Figure 21 can be compared to Figure 17. It shows a distinct difference in the transient area. This difference in position is explained due to the hardware limitation of the system. It is concluded that the real plant is not able to achieve the desired acceleration.
The velocity of the cart-stage was set at 0.20 m/s and met all requirements. The velocity could be increased, but not without changing the control parameters to retain the error within margins.

8.3 Evaluation

Although the system performance mostly met the requirements, there are several things that could be done to further improve the performance of the system.
Firstly, increasing the force capacity of the motor would increase the system accuracy, especially in the transient

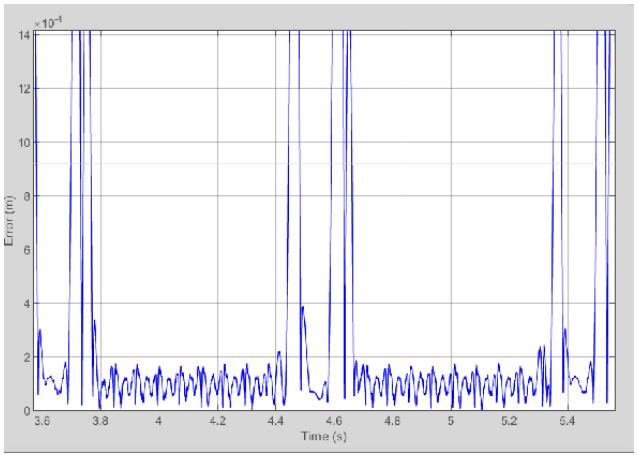

Figure 23: Combined error of the cart and pen stage

part of the trajectory. This could also be achieved by decreasing both the mass of the moving part of the pen stage and decreasing the stiffness of the springs, which would increase the sensitivity of the system to outside forces, including the actuation force.
Secondly, the orientation of the redesign had to be changed. The leaf springs were placed vertically which caused the point of the pen to be lifted of the paper due to shortening. This could either have been fixed by implementing a spring to press the pen on the paper or by changing the orientation of the system. The second option was used.
Also, the system control could be improved by carrying out more accurate measurements of the mechanical parameters of the setup.
Furthermore, the stiffness of the leaf springs in the direction of the parasitic mode shapes can be increased to further decrease unwanted motion in the system.

References

[1] W. Hakvoort, "Specifications for leaf springs," 2019.

[2] prof.dr.ir. A.H. van den Boogaard, "Stijfheid en sterkte 1," 2017.

[3] W. Hakvoort, "Slides digital control," 2019.

[4] F. Grossi, "Matlabs script for logaritmic closed loop nyquist diagram.." `https://nl.mathworks.com/matlabcentral/fileexchange/43768-closed-logarithmic-nyquist-plot`, 2013.

A Measurement plan - Steady state response

A.1 Goal

With this experiment the response of the system to certain voltages will be measured. This test is constructed in order to analyse the linearity of the system and determine the accuracy of the modelled system.

A.2 Method

The steady state response will be tested by supplying the VCM with a varying voltage. The 'Repeating Sequence Stair' Simulink block is used for this. The sensor will measure the displacement. The displacement values after each step has settled will be saved and displayed against the input voltage.

A.3 Measurement parameter

The measurement depends on the following parameters:

- Time between steps, to allow for the system to settle
- Outside interference

A.4 Measurement plan

- **Input a signal comprised of multiple step functions with varying step times.**
  The signal should go from -6 volt to +6 volt, with steps of 1 volt. The time between steps is 2.5 seconds. If the results at certain areas are inconclusive, the step size can be decreased. If the settling time is longer than 2.5 seconds, the time between steps can be increased appropriately.
- **Measure the output**
  The system will be measured at a sampling frequency of 2000 Hz, the same as the system. From the graphs, the displacement at each voltage will be measured after the movement has settled.
- **Repeat to check the consistency of the results**
  If the results are significantly different on a repeat test, run the test 3 times total and take the average displacement at each voltage.
- **Display the results**
  Plot the input voltage against the output displacement. Fit a first degree polynomial for the measured points to check for linearity

A.5 Expected results

The steady state response should give consistent and mostly linear step displacements, with possibly only a slight decrease in displacement caused as the coil of the VCM moves outwards.

A.6 Results

In Figure 24 the result of the measurement is plotted. From this graph it can be seen that for this range the response is indeed linear. There are no results for displacements up to $5mm$, since the output is limited at $\pm 6V$, but since these the displacements are gotten when the system is moving, it is assumed that for the voltage range, the results will be linear.

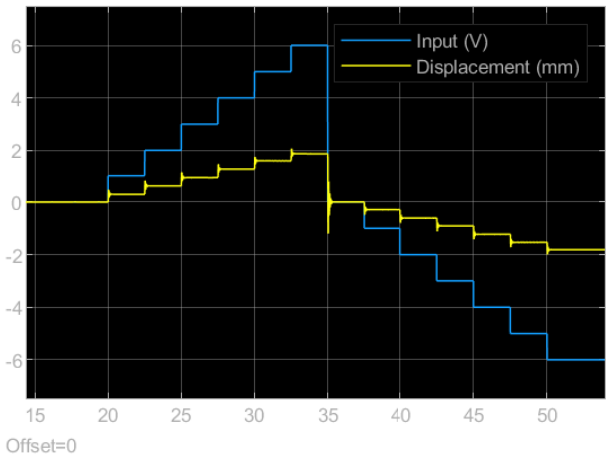

Figure 24: Steady state response

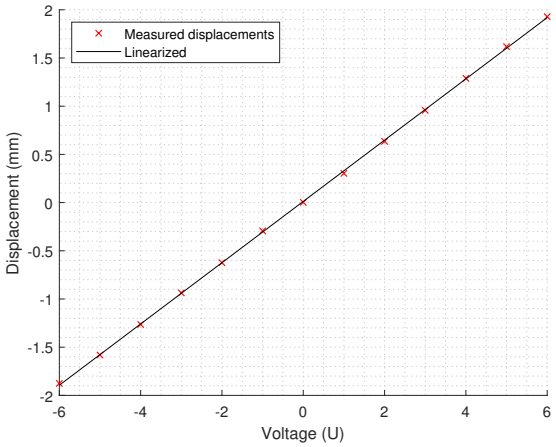

Figure 25: Linearization

B Measurement plan - Frequency response

B.1 Goal

With this experiment the response of the physical plant to certain frequencies will be measured. The aim of this test is to see the several resonance frequencies as well as the available phase margin at the cross over frequency.

B.2 Method

The frequency response of the system is measured by exciting the system with a Chirp signal. This sweeping signal contains all the frequencies in a certain range. The output of the system is measured trough the sensor. And with this the gain and phase of the system can be extracted.

B.3 Measurement parameters

The measurement depends on the following parameters:

- Amplitude of chirp, to reduce noise (SNR)
- Length of measurement (to short yields wrong results)
- Sampling frequency
- Number of repetitions (to reduce random noise)

B.4 Measurement plan

- **Input a chirp signal**
  Choose an amplitude of 1 volt (pen stage) (1/6th the available voltage) and an amplitude of 0.75A (cart stage) (1/5th the available current). If there is too much sensor noise the amplitude can be increased. The range of the sweep should be between 0-4x the expected crossover frequency (Hz). The frequency range for the pen stage should be 0 – 100 Hz. For the cart it should be 0 – 100 Hz as well. The chirp time should not be too short since this will cloud the results (less measuring points per frequency). The longer it takes to complete the chirp the better. Take a time of 15 seconds. The results should be evaluated in step 3.
- **Measure the output**
  Use a sampling frequency of 1000 Hz, 20-50x the expected crossover frequency. This sampling frequency allows us to accurately measure frequencies up to 500 Hz, which is well above the frequency this test reaches.
- **In order to get more accurate results for the higher frequency behaviour the test should be done multiple times**
  After 3 repetitions the results should be evaluated and it should be determined of any of the parameters should be adjusted or if more repetitions are needed.
- **Display the results**
  The results should be two FRF. These results can be compared to the results obtained from the SPACAR transfer functions for the plants. Other results are the natural frequencies an parasitic natural frequencies, and if applicable the available phase margin at the cross over frequency.

B.5 Expected results

The results of the frequency response should have a similar shape as the model from Section 5. But they are expected to deviate from one-another due to friction and other external factors which are not modelled.

B.6 Results

In Figure 26 and Figure 27 the results can be seen. It can be observed that the phase of the carts stage has shifted upwards by 180 degrees. the pen stage response has a higher gain than the model.

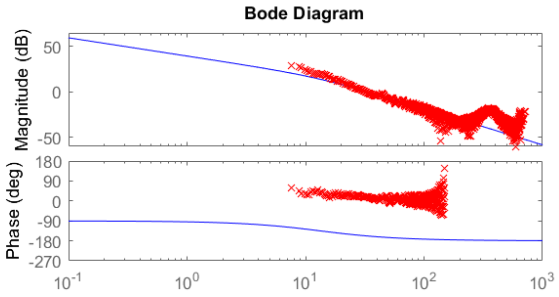

Figure 26: Bode plot of the frequency response of the cart stage(red). and the modelled frequency response (blue)

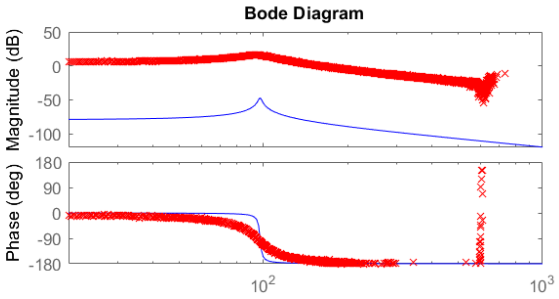

Figure 27: Bode plot of the frequency response of the pen stage (red). and the modelled frequency response (blue)

C Initial Design

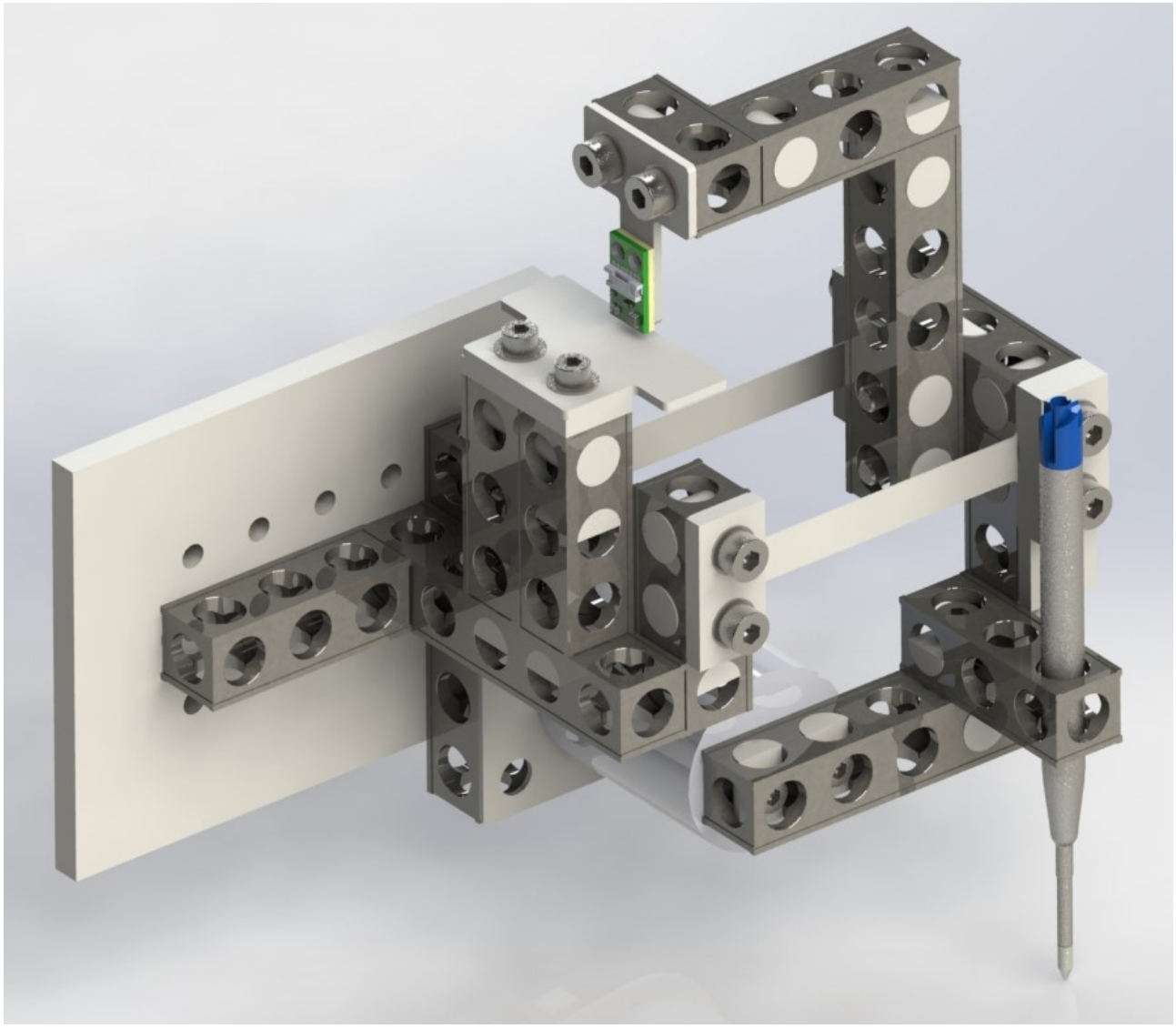

Figure 28: Initial Design

D High order TF [SPACAR]

$$T(s) = \frac{-51.99s^{10} - 3.47 \cdot 10^{5}s^{9} - 8.94 \cdot 10^{11}s^{8} - 2.63 \cdot 10^{15}s^{7} - 3.25 \cdot 10^{21}s^{6} - 5.60 \cdot 10^{22}s^{5}}{s^{1}2 + 9441s^{1}1 + 2.41 \cdot 10^{10}s^{1}0 + 1.23 \cdot 10^{14}s^{9} + 1.47 \cdot 10^{20}s^{8} + 1.22 \cdot 10^{23}s^{7}} \tag{35}$$

$$\frac{+9.93 \cdot 10^{28}s^{4} + 1.99 \cdot 10^{31}s^{3} + 8.78 \cdot 35s^{2} + 5.70 \cdot 37s + 1.07 \cdot 10^{42}}{+2.85 \cdot 10^{28}s^{6} + 4.84 \cdot 10^{30}s^{5} + 1.99 \cdot 10^{35}s^{4} + 1.32 \cdot 10^{37}s^{3} + 2.33 \cdot 10^{41}s^{2} + 1.03 \cdot 10^{42}s + 2.25} \tag{36}$$

E Simulated model bode diagrams

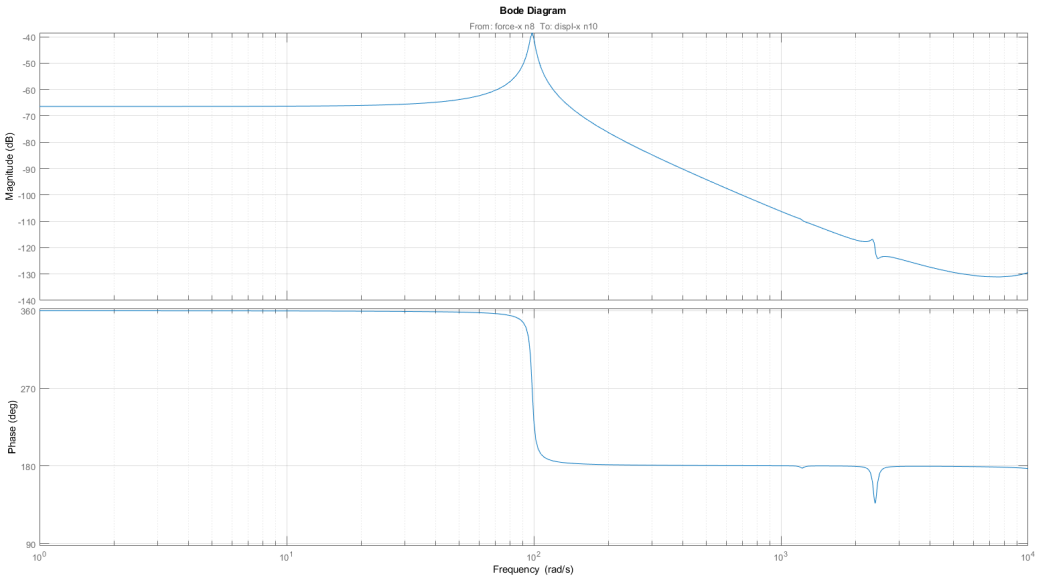

Figure 29: Bode Diagram from SPACAR

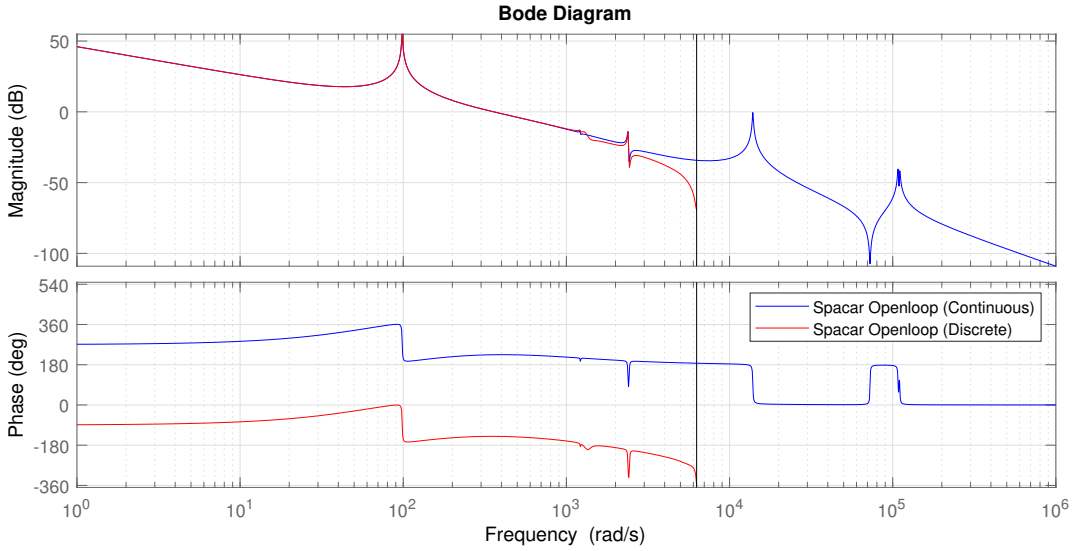

Figure 30: Bode diagram of the simulated plant including controller and feedforward

F Simulink model

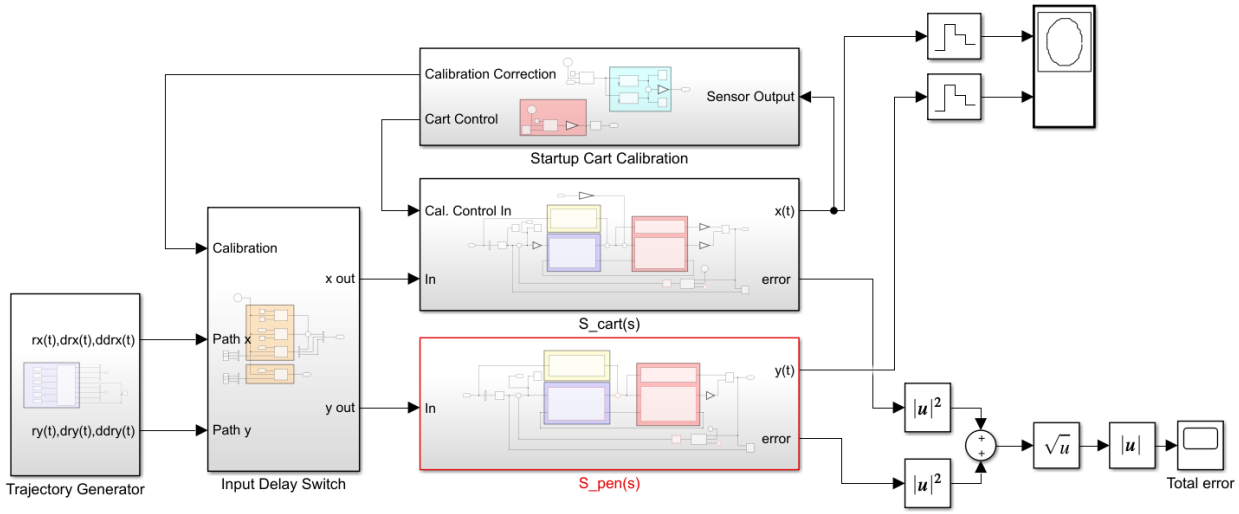

Figure 31: The entire model

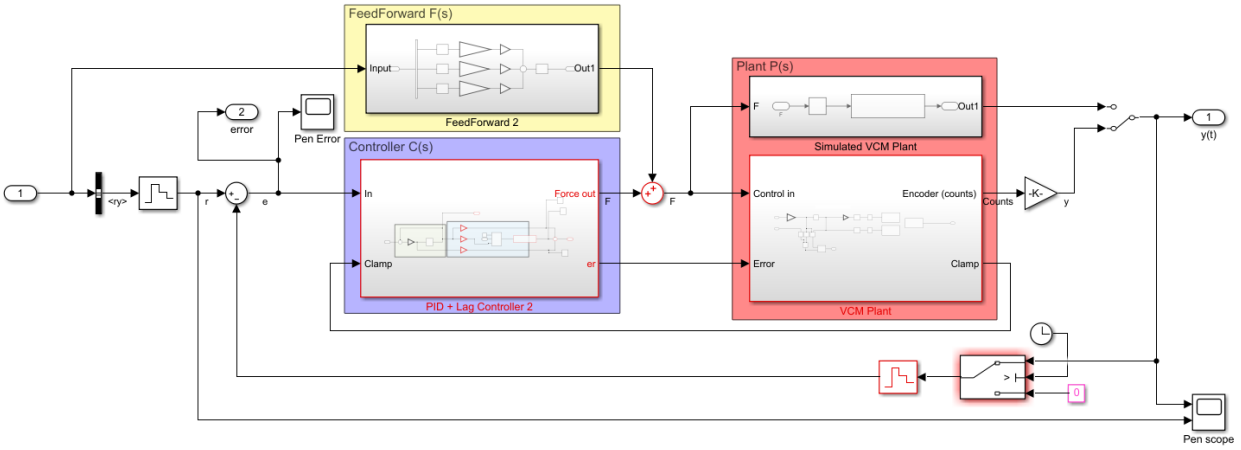

Figure 32: The pen model

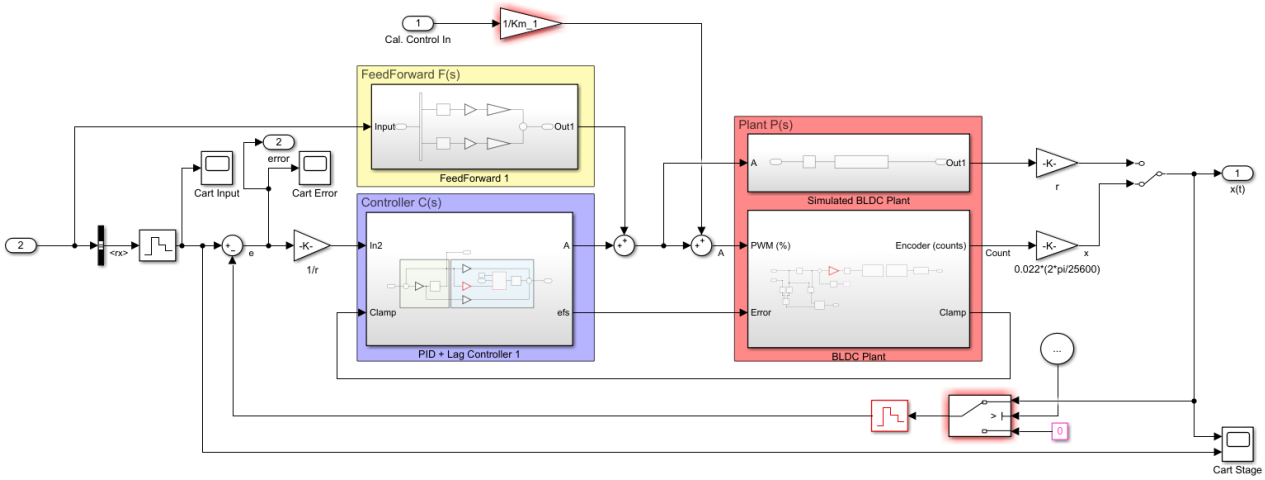

Figure 33: The cart model

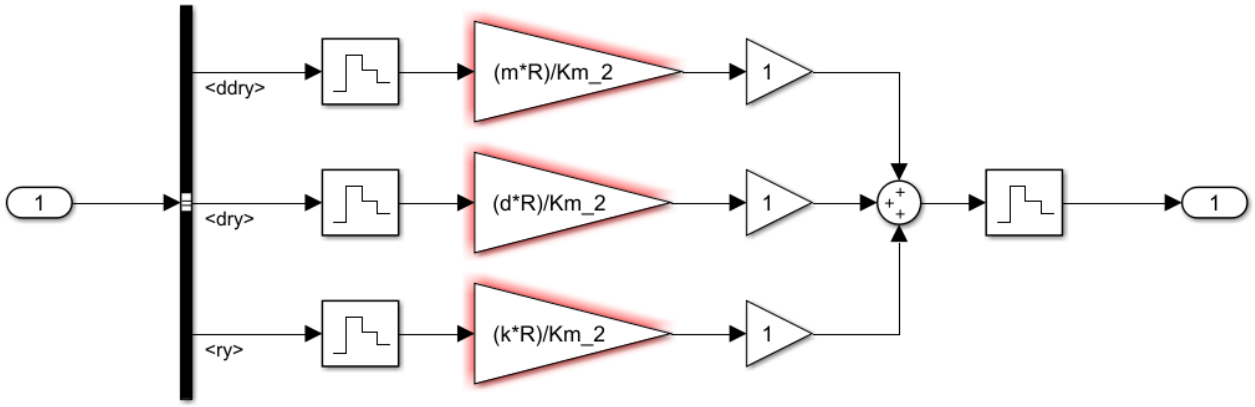

Figure 34: The Feed forward model

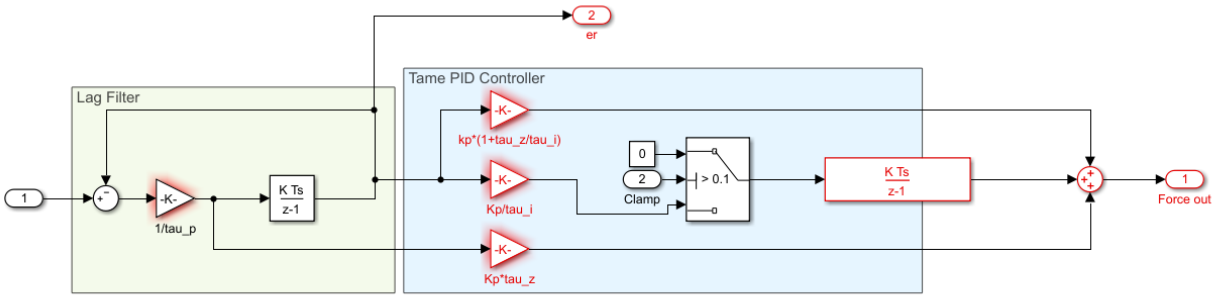

Figure 35: The PID model

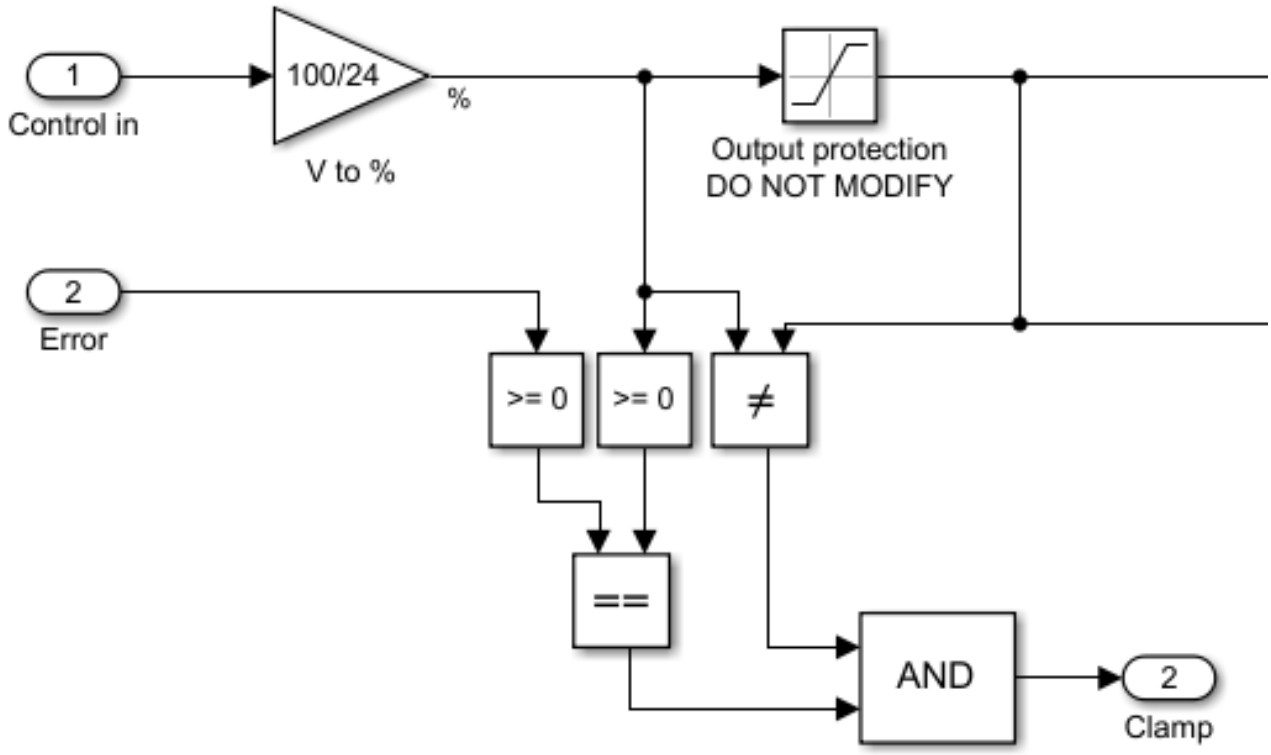

Figure 36: The anti-windup protection

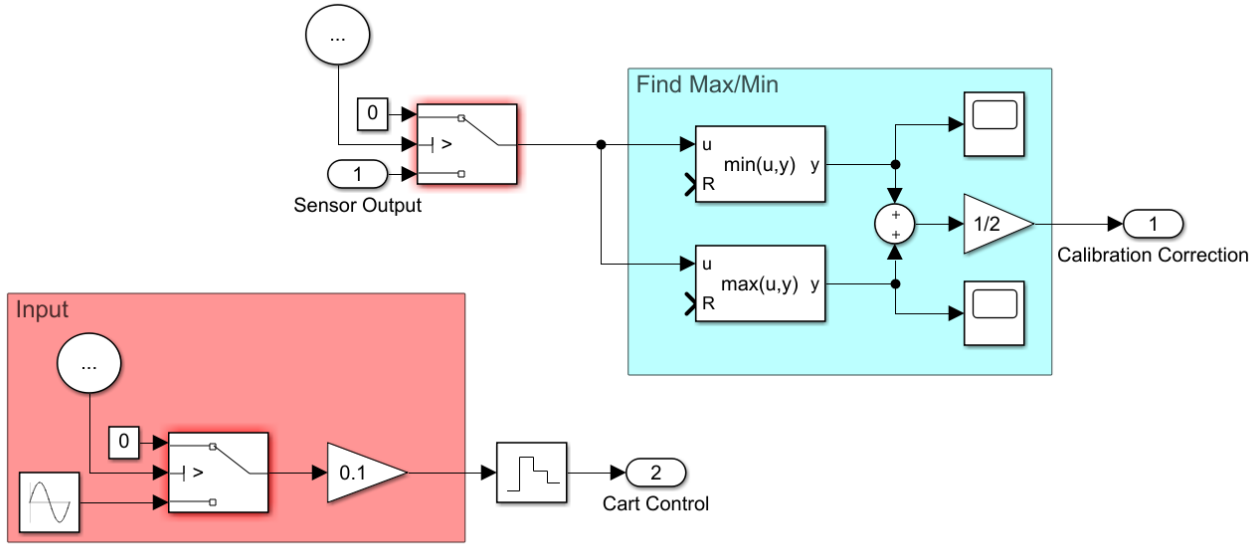

Figure 37: The startup calibration model

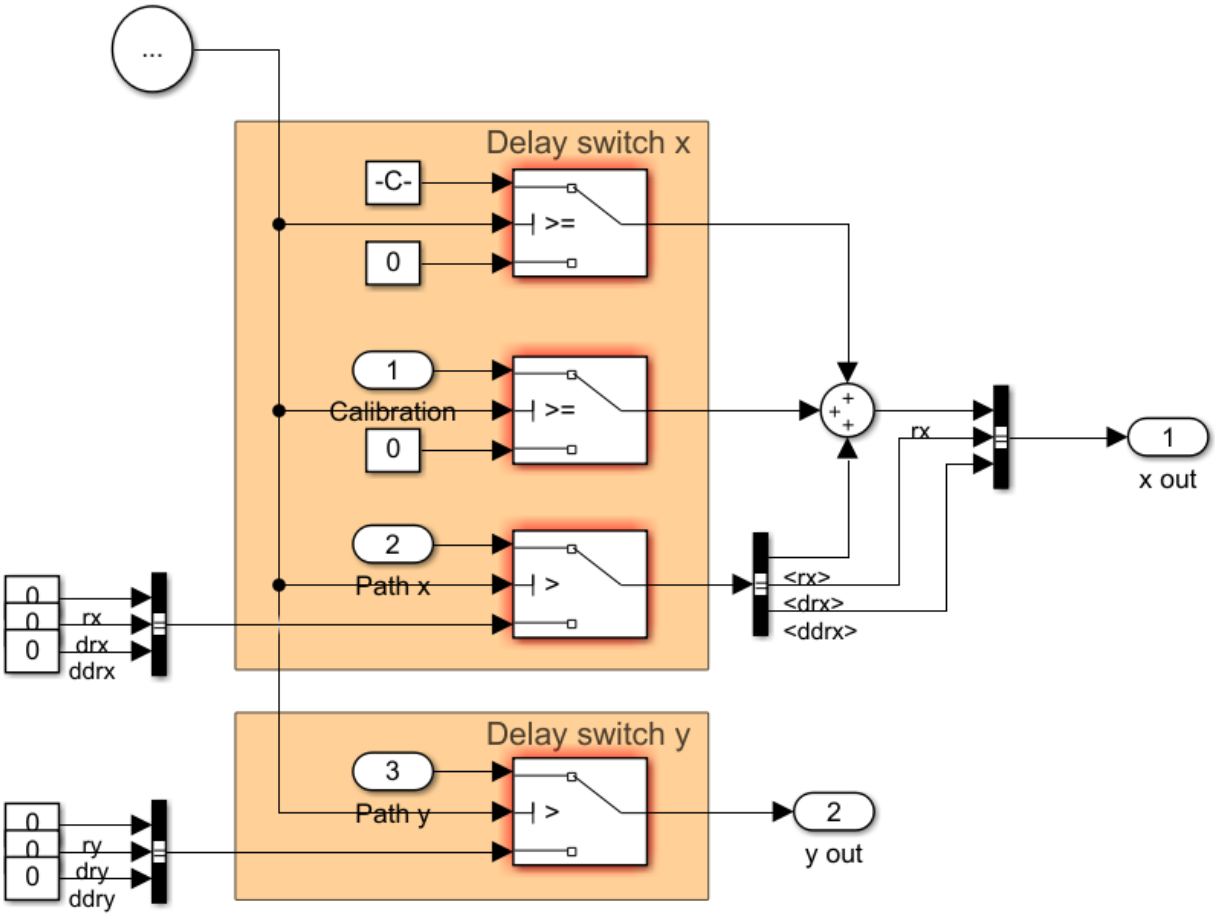

Figure 38: The time switch model